





Multiferroic skyrmions in BiFeO₃Z. Li ¹, T. Chirac ^{1,2}, J. Tranchida ³, V. Garcia ⁴, S. Fusil⁴, V. Jacques,² J.-Y. Chauleau,^{1,*} and M. Viret^{1,*}¹SPEC, CEA, CNRS, Université Paris-Saclay, CEA Saclay, 91191 Gif sur Yvette, France²Laboratoire Charles Coulomb, Université de Montpellier and CNRS, 34095 Montpellier, France³CEA, DES, IRESNE, DEC, SESC, LM2C, F-13108 Saint-Paul-Lez-Durance, France⁴Unité Mixte de Physique CNRS, Thales, Université Paris-Saclay, 91767 Palaiseau, France

(Received 16 December 2022; accepted 22 July 2023; published 3 November 2023)

We show here using atomistic simulations that BiFeO₃ films can be driven through a topological transition when increasing uniaxial anisotropy, which can possibly be achieved by strain. Tuning the anisotropy close to the transition, we show that individual antiferromagnetic skyrmions can reach a very large topological protection. These entities can then be excited by electric fields and spin torque and controllably driven at speeds exceeding 10 km/s.

DOI: [10.1103/PhysRevResearch.5.043109](https://doi.org/10.1103/PhysRevResearch.5.043109)

I. INTRODUCTION

Topology is a prominent concept from which new materials and properties are emerging [1]. In magnetic materials, it often arises as a consequence of the spin-orbit interaction, which couples the electrons' motion to their spin. Broken-inversion symmetry can generate a chiral exchange interaction (Dzyaloshinskii-Moriya interaction, or DMI) that curls spins into noncollinear textures carrying a finite topological charge, such as skyrmions [2]. These concepts applied to the field of spintronics pertain to a new research area coined spin-orbitronics [3]. Ferromagnetic skyrmions obtained in metallic multilayers can be used as ultrasmall bits of magnetic information for mass-data storage [4] and logic operations. However, their application is hindered by several problems: (i) a spin-polarized current pushes the chiral spin texture of skyrmions sideways and the entities eventually get trapped or annihilate on the track edges [5,6]; (ii) the power consumption required to displace them by current pulses is too large [7,8]; and (iii) their displacement speed is limited to about 100 m/s [9]. These drawbacks could be alleviated by working with antiferromagnetic skyrmions [10] that can operate up to 2 orders of magnitude faster than their ferromagnetic counterparts [9,11]. Moreover, using insulators, power consumption could be dramatically reduced, which is the aim of a new field called spin-insulatronics [12].

Usually, magnetic skyrmions are obtained by engineering the interfaces of artificial heterostructures [3,13]. The basic relevant interaction is the DMI that stems from coupling between magnetic atoms in the interface electrical built-in field. It is of the same nature as the more general magnetoelectric

(ME) interaction expressing the gain in energy in the presence of an internal electric field, or polarization, when magnetism is noncollinear [14–16]: $E_{\text{ME}} = \gamma_{\text{ME}} \sum \vec{P} \cdot (\vec{e}_{ij} \times (\vec{S}_i \times \vec{S}_j))$, with γ_{ME} the inhomogeneous ME constant, \vec{P} the polarization, \vec{e}_{ij} the vector linking nearest neighbors, and $\vec{S}_i \times \vec{S}_j$ the cross product of neighboring spins. Therefore, magnetoelectric materials intrinsically possess the relevant interaction for generating skyrmions with an extra functionality; unlike interfaces, it can be toggled by switching the polarization.

Among the relevant materials, BiFeO₃ is archetypical as it is an antiferromagnetic ferroelectric with both ordering temperatures well above room temperature. As such, it has been in the center of the huge revival of so-called “multiferroics” since the early 2000s [17]. A vast literature has emerged to understand their nature [18], the coupling between antiferromagnetism and ferroelectricity [19–22], as well as ways to engineer their properties, e.g., by epitaxial strain [23–25]. In BiFeO₃, the significant coupling between electrical polarization P and AFM order [20–22] forces the existence of a single AFM T domain (of constant AFM staggering order) in a single polarization domain. This simplifies the domain structure of the AFM order, leaving only three possible cycloids or three possible AFM S domains (when cycloids are destabilized by strain) [26]. The possibilities offered by thin-film technologies and strain engineering are exciting, but it is thus far unclear which internal parameters should be tailored to produce and control individual skyrmions. The goal of the present paper is to pave the way to experimentally achieve this, based on realistic modeling of BiFeO₃.

II. MODELING OF BiFeO₃ SPIN TEXTURE

Modeling of antiferromagnetic textures requires an atomistic simulation because magnetization is non-zero and constant only at the single atomic scale. Generally, appropriate codes are dynamic ones where the two AF sublattices are described by a set of two coupled Landau-Lifshitz-Gilbert (LLG) precession equations [27–29]. Any perturbation results in coupled motion of individual spins and the existence of

*jean-yves.chauleau@cea.fr; michel.viret@cea.fr

TABLE I. Parameters of the microscopic spin model of BiFeO₃.

Parameter	J_1	J_2	D_1	D_2	K_1	K_3	α
Value in meV	-5.3	-0.2	0.18	0.06	0.004	6×10^{-6}	0.001

damping makes the system reach a stable static state after some time. This is quite heavy on calculation time if one wants to simulate a reasonable volume, say 10^6 spins. Here, a specific program was written to process the calculation in parallel on GPUs. It is based on following the time evolution using the LLG equation with the following relevant Hamiltonian:

$$\begin{aligned}
\mathcal{H} = & J_1 \sum_{\langle i,j \rangle} \mathbf{S}_i \cdot \mathbf{S}_j + J_2 \sum_{\langle i,j \rangle'} \mathbf{S}_i \cdot \mathbf{S}_j \\
& + D_1 \sum_{\langle i,j \rangle} \left(\mathbf{z}' \times \frac{\mathbf{e}_{ij}}{a} \right) \cdot (\mathbf{S}_i \times \mathbf{S}_j) \\
& + D_2 \sum_{\langle i,j \rangle} (-1)^{h_{ij}} \mathbf{z}' \cdot (\mathbf{S}_i \times \mathbf{S}_j) \\
& - K_1 \sum_i (\mathbf{z}' \cdot \mathbf{S}_i)^2 \\
& - K_3 S^6 \sum_i \sin^6 \theta_i \cos^6 \phi_i,
\end{aligned}$$

with J_1 and J_2 the exchange interactions between, respectively, first and second neighbors, D_1 the inhomogeneous magnetoelectric constant, and D_2 the DMI interaction. K_1 and K_3 are the uniaxial (along P , i.e., [111]) and in-plane (perpendicular to P) anisotropy constants, respectively, $S_{i,j}$ are the Fe spins, θ and ϕ are the out-of-plane (111) and in-plane angles, respectively, taken around \mathbf{z}' , i.e., the [111] direction. These parameters have been calculated [30] and measured for BiFeO₃ and we use here their generally accepted values [31], given in Table I. The evolution of the simulation is driven by the LLG equation:

$$\begin{aligned}
\frac{d\hat{\mathbf{s}}}{dt} &= \boldsymbol{\omega}_\Sigma \times \hat{\mathbf{s}} - \alpha \frac{d\hat{\mathbf{s}}}{dt} \times \hat{\mathbf{s}} \quad \text{with} \\
\boldsymbol{\omega}_\Sigma &= \gamma \mu_0 \mathbf{H}_\Sigma + \hat{\mathbf{s}} \times \boldsymbol{\omega}_\tau = -\frac{1}{\hbar S} \frac{\partial \mathcal{H}}{\partial \hat{\mathbf{s}}} + \hat{\mathbf{s}} \times \boldsymbol{\omega}_\tau,
\end{aligned}$$

where $\hat{\mathbf{s}} = \mathbf{S}/S$ is a unit vector with spin taken to be 2.5, $\boldsymbol{\omega}_\Sigma$ the derivative of the Hamiltonian \mathcal{H} including the spin-transfer torque $\boldsymbol{\omega}_\tau$ (addressed below), and α is the damping parameter (see Table I).

The calculation is carried out by solving the differential equation numerically using the Euler method:

$$\frac{d\hat{\mathbf{s}}}{dt} = \boldsymbol{\omega}_{\text{eff}} \times \hat{\mathbf{s}} \quad \text{with} \quad \boldsymbol{\omega}_{\text{eff}} = \frac{1}{1 + \alpha^2} (\boldsymbol{\omega}_\Sigma - \alpha \boldsymbol{\omega}_\Sigma \times \hat{\mathbf{s}}).$$

It is first instructive to simulate a piece of bulk BiFeO₃ (Fig. 1) using periodic boundary conditions. As expected, the long-range cycloid is obtained along one of the three degenerate [1-10]-type directions. Note that these are set because of the threefold in-plane anisotropy term (K_3). Moreover, the second (alternate) DMI term (D_2) leads to a concomitant spin-density wave locked on the ME-induced cycloid. Interestingly, this gives rise to a small magnetic stray field that makes possible its detection in real space [32]. These basic checks made with 5×10^5 spins validate the parameters used for the Hamiltonian.

III. ANTIFERROMAGNETIC SKYRMION IN BiFeO₃

A. Stability

The next step is now to study if a skyrmion can be stabilized in a BiFeO₃ slab. We chose to nucleate numerically an individual skyrmion in a box with periodic boundary conditions in all directions and let the numerical simulations relax to their equilibrium state. In order for the calculation to be unaffected by the boundaries, we have varied the box size and observe that they converge to a similar energy for a size above 120 nm. The relaxed skyrmion, shown in Fig. 2(a), is 28 nm in size for $K_1 = 0.012$ meV, shrinking noticeably when anisotropy increases further. It is of hybrid nature as the spin winding generates an extra polarization in virtue of the spin-current model: $\bar{P}_{\text{ME}} \sim \bar{e}_{ij} \times (\bar{S}_i \times \bar{S}_j)$. Note that this electrical part is not chiral as it is generated by the spin chirality in a direction parallel to \bar{P} , hence purely along [111] [Fig. 2(b)]. This could represent a big advantage for the detection of such chiral objects. Moreover, we have also let the simulations converge starting from different initial conditions including a collinear AFM state and an infinite cycloid. The

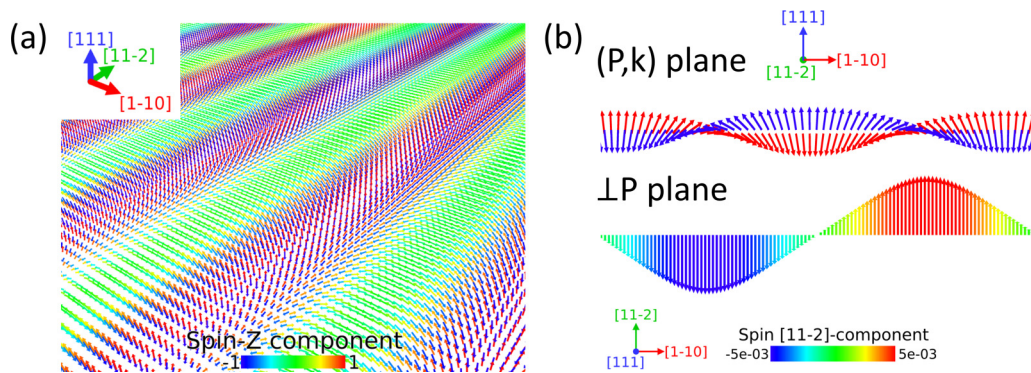


FIG. 1. Simulated bulk cycloidal state in BiFeO₃. (a) ME and exchange interactions are responsible for the 64-nm-period AFM cycloid obtained as the ground state of system. A small concomitant spin-density wave is induced in the perpendicular direction by alternating DMI due to antiphase rotation of oxygen atoms along [111]. This is better seen in projections on relevant planes in (b).

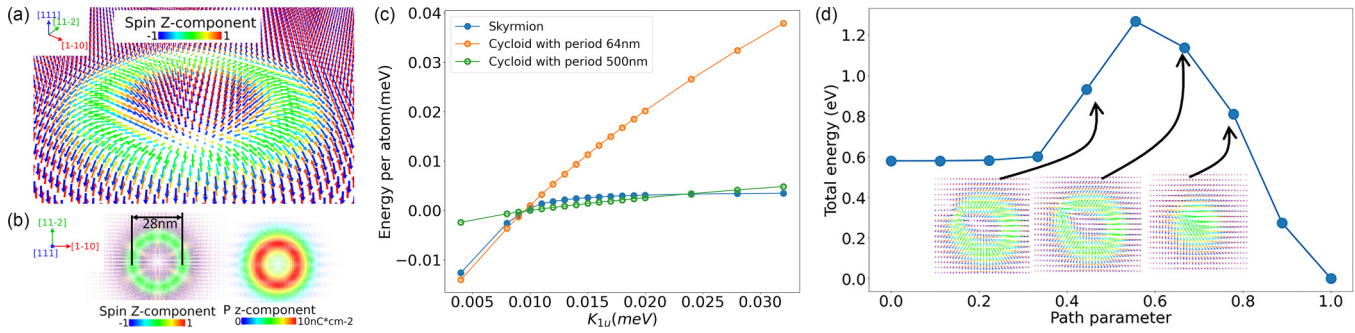


FIG. 2. Metastability of skyrmionic states. (a) Relaxed AFM skyrmion state for an anisotropy $K_1 = 0.012$ eV (only 1 out of 24 spin vectors is represented in this figure and in the following ones). (b) [111] projection of the spin component (left) and associated electric polarization (right). (c) Phase diagram (energy vs anisotropy) where zero is defined as the collinear AFM state. Obtained ground states are cycloids below $K = 0.010$ meV and a collinear AFM state above. (d) Unwinding of a skyrmion as obtained with the GNEB technique following minimum-energy path. Skyrmions are metastable but, once nucleated, they are protected by a large energy barrier of 0.7 eV of topological nature.

results show that the energy of the skyrmion state is never the lowest. Indeed, when the anisotropy K_1 varies, the cycloid and the collinear AFM are found to be ground state at low K_1 and above $K_1 = 0.010$ meV, respectively [Fig. 2(c), where the zero energy is taken as that of the G -type AFM order]. However, for K_1 slightly above 0.010 meV and all the way to 0.020 meV, a skyrmion can be successfully relaxed [Fig. 2(a)] for a simulation with periodic boundary conditions (a similar object is obtained in a 4-nm-thick BFO layer with free-boundary conditions in the [111] direction), if the initial state already has the right topology. The nucleated skyrmion in such a material is therefore metastable. This can be verified by a procedure called GNEB [33,34] implemented in the Large-scale Atomic/Molecular Massively Parallel Simulator LAMMPS [35,36]. It is presented in Fig. 2(d) for $K_1 = 0.012$ meV, where the minimum-energy path is computed for skyrmion annihilation. It is found hereby that in order to unwind the topological structure, an energy barrier of the order of 0.7 eV has to be overcome. This is much above what temperature can do and we conclude that once nucleated, these entities are very stable in BiFeO₃. The main requirement here is that the uniaxial anisotropy has to be increased (by a factor of 3) compared to that of bulk samples. Epitaxial strain is probably the right strategy to achieve this, as it was already shown that different antiferromagnetic ground states (collinear AFM and different cycloid types) can be obtained when BiFeO₃ is grown on different substrates with different orientations [22,23,25,37]. Moreover, anisotropy is the parameter primarily affected by strain in BFO while exchange and DMI interactions vary slowly [25].

B. Nucleation

In order to go beyond the mere stability arguments, it is essential to find the right stimulus to control the AFM skyrmionic texture both to nucleate and move the entities. The prime candidate for this is spin-transfer torque (STT) [11,27,38]. Since our material is insulating, out-of-equilibrium angular momentum has to be injected from another layer through an interface, for instance an adjacent conducting Pt layer traversed by a large current. Experimentally, it appears that this has never been achieved

because the required current densities are so large that Joule heating has more effect than injected angular momentum. An alternative to inject the required spin densities with limited Joule effect relies on the ultrafast demagnetization of an adjacent ferromagnetic layer using a femtosecond optical laser pulse [Fig. 3(a)]. This is the main mechanism envisioned in the present paper, taking reasonable spin bursts as measured experimentally [39]. Photoconductive switches may also be used to generate spin currents at picosecond timescales [40]. For computational purposes, the dampinglike Slonczewski spin-transfer torque is introduced in the equation of motion as

$$\omega_\tau \simeq \frac{G a^3}{l n_s} \mathbf{j}_s,$$

with G the spin transparency at the interface, a the lattice constant, n_s the number of magnetic atoms per unit cell, l the thickness of the layer, and \mathbf{j}_s the spin current expressed in $\mu_B \text{ m}^{-2} \text{ s}^{-1}$. ω_τ has the dimension of a frequency. Here, we take $G = 0.1$, $a = 0.396$ nm, $n_s = 5 \mu_B$ per unit cell, $l = 5$ nm, and $j_s = 6 \times 10^{31} \mu_B \text{ m}^{-2} \text{ s}^{-1}$, which leads to $\omega_\tau = 14.9$ GHz, corresponding to 9.8×10^{-3} meV in energy per atom.

In the case of a homogeneous AFM domain, different behaviors can occur depending on the orientation and strength of the STT with respect to the Néel vector [28,29]. In particular, during a subpicosecond STT pulse applied perpendicular to it, the spins tilt towards the STT direction, accumulating energy and gaining magnetization; then, they relax by gyrating along the generated magnetization direction on picosecond timescales. If the torque overcomes the anisotropy energy barrier, and the total angular momentum injected is sufficient, the spins eventually relax to another stable direction.

Therefore, STT can be used both for the excitation and for the nucleation of the topological entities. It is actually a nucleation mechanism of choice as it can be applied locally. Here, we numerically attempt the experiment on a 240-nm \times 240-nm area of a homogeneous AFM domain. Interestingly, applying a 200-fs-long STT pulse along the [11-2] direction with an amplitude of $j_s = 4.1 \times 10^{32} \mu_B \text{ m}^{-2} \text{ s}^{-1}$ generates a closed domain wall that relaxes to a skyrmion state after 66 ps, as shown in Fig. 3. This spin current is 6 times higher than that

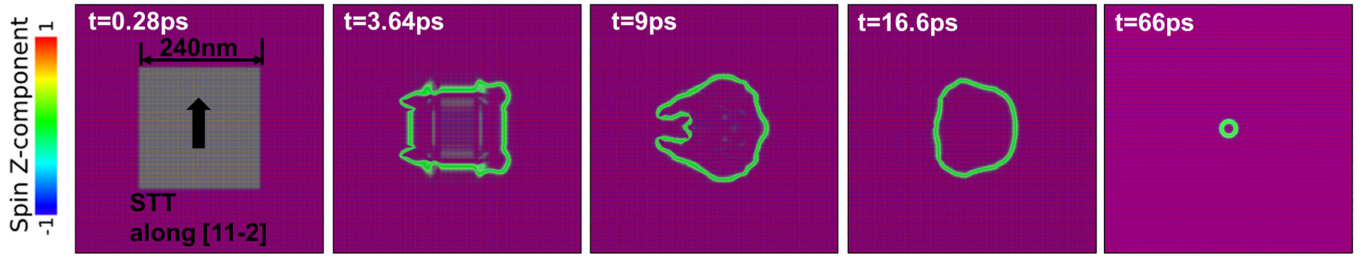


FIG. 3. Skyrmion nucleation induced by spin-transfer torque. A 200 fs long STT pulse is applied along [11-2] with $j_s = 4.1 \times 10^{32} \mu_B \text{ m}^{-2} \text{ s}^{-1}$ on area of $240 \text{ nm} \times 240 \text{ nm}$. As shown in $t = 0.28$ -ps snapshot this nucleates a closed domain wall that relaxes to a skyrmion. STT is applied starting at $t = 0$ ps.

reported in experiments, but successful skyrmion nucleation might be experimentally achieved for smaller values given the (rather conservative) assumption of an interface spin transparency of $G = 0.1$. However, such large threshold values are not so surprising as the topological protection acts both ways and thus impedes nucleation. These are nevertheless reasonable conditions to attempt nucleating a skyrmion in BiFeO_3 , especially if one could use another parameter like temperature to temporarily decrease the energy barrier.

It is also tempting to use an electric-field pulse for nucleation purposes as adding a field to P should amplify the magnetoelectric effect and promote cycloidal rotation. However, we find that this does not generate the appropriate skyrmion for any reasonable field value applied on a 100-nm spot. This is understandable as the huge 1.2-eV energy barrier of Fig. 2(d) (to go from the uniform AFM state to the skyrmion) corresponds to values of E of 10 times P unachievable in real life. Attempting a periodic resonant excitation, we also failed to nucleate a skyrmion even for a field amplitude of 100 MV/cm. Therefore, an electric field alone is not adequate for nucleation.

C. Dynamics

Using STT is therefore the best technique to control the AFM order even in a multiferroic AFM material. We find that this is especially efficient to trigger the dynamics of preexisting skyrmions in a BiFeO_3 layer. Here, our atomistic simulations are essential because as the angle of angular

momentum accumulation and local spins vary in space, it is hard to simply predict the possible distortion and motion of a topological entity. Previous works on pure antiferromagnets have addressed part of the questions arising here [11,41–43] but multiferroics have not been tackled yet. Our geometry is similar to that of Zhang *et al.* [11], but our angular momentum is injected in very short (20 or 200 fs) and intense bursts, and in a direction that can be set at will by an external magnetic field. It is not our intention here to study in detail the different excitation modes triggered in the skyrmion, but one can note that the entity mainly responds at its internal frequency of 0.65 THz, with an intensity proportional to the excitation amplitudes [Fig. 4(a)]. More interestingly, a spin burst along the [1-10] direction does trigger skyrmion motion in a direction perpendicular to that of the injected spins [Fig. 4(b)]. In fact, the short pulses transfer some momentum to the skyrmion, which, in virtue of its mass, inertia, and damping, is set in motion for some picoseconds as shown in Fig. 4(c). Its initial velocity can be in the range of 10 km/s and it averages to a few km/s over the 10 ps it takes before stopping. In the vision of turning this phenomenon into an ultrafast memory element, the stoppage time could be further reduced using a different pulse shape (a 1-ps bipolar pulse could possibly allow for an appropriate THz writing).

Since required excitations are smaller for exciting skyrmions than for nucleating them, we again attempted electric-field pulses. Indeed, an electric field applied along the direction of P either adds to or subtracts from the intrinsic magnetoelectric effect which either contracts or expands the

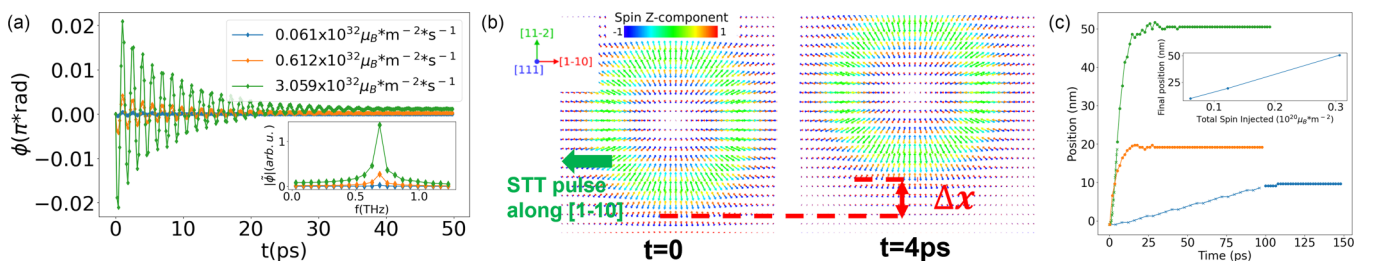


FIG. 4. Skyrmion dynamics induced by spin-transfer torque. (a) Skyrmion dynamics induced by a 20-fs [111] spin-transfer torque pulse (FFT in inset), and (b) its motion resulting from a $[-110]$ pulse with 200-fs duration. A maximum initial velocity over 10 km/s can be reached in a direction perpendicular to that of the injected spins without destroying the skyrmion. (c) Skyrmion motion for parameters mimicking three different experiments: 100-ps-long spin injection from Pt with $j_s = 0.06 \times 10^{30} \mu_B \text{ m}^{-2} \text{ s}^{-1}$ (blue line), STT generated from ultrafast demagnetization of a ferromagnetic adjacent layer applied for 0.2 ps with $j_s = 61 \times 10^{30} \mu_B \text{ m}^{-2} \text{ s}^{-1}$ (orange line), and a 5-ps-long STT pulse delivered by a photoconductive switch with $j_s = 6 \times 10^{30} \mu_B \text{ m}^{-2} \text{ s}^{-1}$ (green line). Crosses and filled circles represent positions, respectively, during and after STT pulses. The inset shows that the final position scales linearly with the total amount of spins injected.

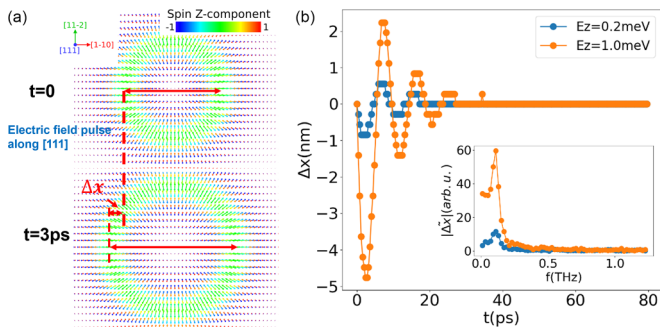


FIG. 5. Electric-field induced skyrmion dynamics. (a) Breathing mode induced by a [111] electric pulse where the mode frequency (b) is obtained at 0.11 THz (FFT is in inset). The applied field is overly large (500 MV/cm) in order to better visually see the effect on the figure, but smaller fields give similar qualitative results.

skyrmion. This triggers a breathing mode beating at 0.11 THz as can be seen in Fig. 5.

IV. CONCLUSION

To conclude, we have explored the conditions to drive BiFeO₃ towards a topological transition. We found that with a slightly enhanced uniaxial anisotropy that could be induced

using strain, individual antiferromagnetic skyrmions are protected by a large topological barrier. Using spin-transfer torque alone, nucleation is hard to achieve with experimentally available intensities (at least within our simple model), but perhaps not impossible with the help of temperature to reduce the energy barrier. In any case, STT is adequate to excite and even push preexisting skyrmions with speeds faster than 10 km/s. Therefore, our simulation work should trigger experimental studies to reach the conditions to produce skyrmions in BiFeO₃ and use these entities as advantageous alternatives to their ferromagnetic counterparts regarding their faster dynamics and simpler linear motion.

ACKNOWLEDGMENTS

We are thankful for support from the European Union's Horizon 2020 research and innovation programme under Grant Agreement No. 964931 (TSAR) and Grant No. 866267 (EXAFONIS), and the DARPA TEE program. We also acknowledge funding from the Agence Nationale pour la Recherche (ANR), project TATOO (Ref. No. ANR-21-CE09-0033). This work was also supported by a public grant overseen by the ANR as part of the "Investissement d'Avenir" programme (LABEX NanoSaclay, SPICY Ref. No. ANR-10-LABX-0035). We also thank Bertrand Dupé, Sebastian Meyer, and Joo-Von Kim for stimulating discussions.

- [1] F. D. M. Haldane, Nobel Lecture: Topological quantum matter, *Rev. Mod. Phys.* **89**, 040502 (2017).
- [2] A. Fert, N. Reyren, and V. Cros, Magnetic skyrmions: Advances in physics and potential applications, *Nat. Rev. Mater.* **2**, 17031 (2017).
- [3] A. Soumyanarayanan, N. Reyren, A. Fert, and C. Panagopoulos, Emergent phenomena induced by spin-orbit coupling at surfaces and interfaces, *Nature (London)* **539**, 509 (2016).
- [4] A. Fert, V. Cros, and J. Sampaio, Skyrmions on the track, *Nat. Nanotechnol.* **8**, 152 (2013).
- [5] W. Jiang *et al.*, Direct observation of the skyrmion Hall effect, *Nat. Phys.* **13**, 162 (2017).
- [6] K. Litzius *et al.*, Skyrmion Hall effect revealed by direct time-resolved X-ray microscopy, *Nat. Phys.* **13**, 170 (2017).
- [7] Y. Liu *et al.*, Voltage-Driven High-Speed Skyrmion Motion in a Skyrmion-Shift Device, *Phys. Rev. Appl.* **11**, 014004 (2019).
- [8] S. Woo *et al.*, Observation of room-temperature magnetic skyrmions and their current-driven dynamics in ultrathin metallic ferromagnets, *Nat. Mater.* **15**, 501 (2016).
- [9] C. Jin, C. Song, J. Wang, and Q. Liu, Dynamics of antiferromagnetic skyrmion driven by the spin Hall effect, *Appl. Phys. Lett.* **109**, 182404 (2016).
- [10] J. Barker and O. A. Tretiakov, Static and Dynamical Properties of Antiferromagnetic Skyrmions in the Presence of Applied Current and Temperature, *Phys. Rev. Lett.* **116**, 147203 (2016).
- [11] X. Zhang, Y. Zhou, and M. Ezawa, Antiferromagnetic skyrmion: Stability, creation and manipulation, *Sci. Rep.* **6**, 24795 (2016).
- [12] A. Brataas, B. van Wees, O. Klein, G. de Loubens, and M. Viret, Spin insulatronics, *Phys. Rep.* **885**, 1 (2020).
- [13] A. Fert and P. M. Levy, Role of Anisotropic Exchange Interactions in Determining the Properties of Spin-Glasses, *Phys. Rev. Lett.* **44**, 1538 (1980).
- [14] H. Katsura, N. Nagaosa, and A. V. Balatsky, Spin Current and Magnetoelectric Effect in Noncollinear Magnets, *Phys. Rev. Lett.* **95**, 057205 (2005).
- [15] M. Mostovoy, Ferroelectricity in Spiral Magnets, *Phys. Rev. Lett.* **96**, 067601 (2006).
- [16] A. M. Kadomtseva, A. K. Zvezdin, Y. F. Popov, A. P. Pyatakov, and G. P. Vorob'ev, Space-time parity violation and magnetoelectric interactions in antiferromagnets, *JETP Lett.* **79**, 571 (2004).
- [17] M. Fiebig, Revival of the magnetoelectric effect, *J. Phys. D* **38**, R123 (2005).
- [18] G. Catalan and J. F. Scott, Physics and applications of bismuth ferrite, *Adv. Mater.* **21**, 2463 (2009).
- [19] I. Sosnowska, T. Peterlin-Neumaier, and E. Steichele, Spiral magnetic ordering in bismuth ferrite, *J. Phys. C: Solid State Phys.* **15**, 4835 (1982).
- [20] I. Sosnowska and A. K. Zvezdin, Origin of the long period magnetic ordering in BiFeO₃, *J. Magn. Magn. Mater.* **140-144**, 167 (1995).
- [21] D. Lebeugle *et al.*, Electric-Field-Induced Spin Flop in BiFeO₃ Single Crystals at Room Temperature, *Phys. Rev. Lett.* **100**, 227602 (2008).
- [22] A. Haykal *et al.*, Antiferromagnetic textures in BiFeO₃ controlled by strain and electric field, *Nat. Commun.* **11**, 1704 (2020).
- [23] D. Sando *et al.*, Crafting the magnonic and spintronic response of BiFeO₃ films by epitaxial strain, *Nat. Mater.* **12**, 641 (2013).

- [24] D. Sando, A. Barthélémy, and M. Bibes, BiFeO₃ epitaxial thin films and devices: Past, present and future, *J. Phys.: Condens. Matter* **26**, 473201 (2014).
- [25] Z. Chen *et al.*, Complex strain evolution of polar and magnetic order in multiferroic BiFeO₃ thin films, *Nat. Commun.* **9**, 3764 (2018).
- [26] J.-Y. Chauleau, E. Haltz, C. Carrétéro, S. Fusil, and M. Viret, Multi-stimuli manipulation of antiferromagnetic domains assessed by second-harmonic imaging, *Nat. Mater.* **16**, 803 (2017).
- [27] R. Cheng, J. Xiao, Q. Niu, and A. Brataas, Spin Pumping and Spin-Transfer Torques in Antiferromagnets, *Phys. Rev. Lett.* **113**, 057601 (2014).
- [28] R. Cheng, M. W. Daniels, J.-G. Zhu, and D. Xiao, Ultrafast switching of antiferromagnets via spin-transfer torque, *Phys. Rev. B* **91**, 064423 (2015).
- [29] T. Chirac, J.-Y. Chauleau, P. Thibaudeau, O. Gomonay, and M. Viret, Ultrafast antiferromagnetic switching in NiO induced by spin transfer torques, *Phys. Rev. B* **102**, 134415 (2020).
- [30] B. Xu, S. Meyer, M. J. Verstraete, L. Bellaiche, and B. Dupé, First-principles study of spin spirals in the multiferroic BiFeO₃, *Phys. Rev. B* **103**, 214423 (2021).
- [31] R. S. Fishman, The microscopic model of BiFeO₃, *Physica B* **536**, 115 (2018).
- [32] I. Gross *et al.*, Real-space imaging of non-collinear antiferromagnetic order with a single-spin magnetometer, *Nature (London)* **549**, 252 (2017).
- [33] P. F. Bessarab, V. M. Uzdin, and H. Jónsson, Method for finding mechanism and activation energy of magnetic transitions, applied to skyrmion and antivortex annihilation, *Comput. Phys. Commun.* **196**, 335 (2015).
- [34] A. V. Ivanov, D. Dagbartsson, J. Tranchida, V. M. Uzdin, and H. Jónsson, Efficient optimization method for finding minimum energy paths of magnetic transitions, *J. Phys.: Condens. Matter* **32**, 345901 (2020).
- [35] J. Tranchida, S. J. Plimpton, P. Thibaudeau, and A. P. Thompson, Massively parallel symplectic algorithm for coupled magnetic spin dynamics and molecular dynamics, *J. Comput. Phys.* **372**, 406 (2018).
- [36] A. P. Thompson *et al.*, LAMMPS - A flexible simulation tool for particle-based materials modeling at the atomic, meso, and continuum scales, *Comput. Phys. Commun.* **271**, 108171 (2022).
- [37] F. Bai *et al.*, Destruction of spin cycloid in (111)c-oriented BiFeO₃ thin films by epitaxial constraint: Enhanced polarization and release of latent magnetization, *Appl. Phys. Lett.* **86**, 032511 (2005).
- [38] H. V. Gomonay and V. M. Loktev, Spin transfer and current-induced switching in antiferromagnets, *Phys. Rev. B* **81**, 144427 (2010).
- [39] T. Kampfrath *et al.*, Terahertz spin current pulses controlled by magnetic heterostructures, *Nat. Nanotechnol.* **8**, 256 (2013).
- [40] K. Jhuria *et al.*, Spin-orbit torque switching of a ferromagnet with picosecond electrical pulses, *Nat. Electron.* **3**, 680 (2020).
- [41] V. P. Kravchuk, O. Gomonay, D. D. Sheka, D. R. Rodrigues, K. Everschor-Sitte, J. Sinova, J. van den Brink, and Y. Gaididei, Spin eigenexcitations of an antiferromagnetic skyrmion, *Phys. Rev. B* **99**, 184429 (2019).
- [42] X. Zhang, Y. Zhou, and M. Ezawa, Magnetic bilayer-skyrmions without skyrmion Hall effect, *Nat. Commun.* **7**, 10293 (2016).
- [43] H. Velkov *et al.*, Phenomenology of current-induced skyrmion motion in antiferromagnets, *New J. Phys.* **18**, 075016 (2016).